JPNT 6(2), 43-51 (2017)
https://doi.org/10.11003/JPNT.2017.6.2.43

JPNT Journal of Positioning, Navigation, and Timing

Performance Analysis of Array Processing Techniques for GNSS Receivers under Array Uncertainties

Sangwoo Lee[1], Moon-Beom Heo[1], Cheonsig Sin[2], Sunwoo Kim[3†]

[1]Satellite Navigation Team, Korea Aerospace Research Institute, Daejeon 34133, Korea
[2]Department of Satellite Wireless Convergence Research, Electronics and Telecommunications Research Institute, Daejeon 34129, Korea
[3]Department of Electronics Engineering, Hanyang University, Seoul 04763, Korea

ABSTRACT

In this study, the effect of the steering vector model mismatch due to array uncertainties on the performance of array processing was analyzed through simulation, along with the alleviation of the model mismatch effect depending on array calibration. To increase the reliability of the simulation results, the actual steering vector of the array antenna obtained by electromagnetic simulation was used along with the Jahn's channel model, which is an experimental channel model. Based on the analysis of the power spectrum for each direction, beam pattern, and the signal-to-interference-plus-noise ratio of the beamformer output, the performance deterioration of array processing due to array uncertainties was examined, and the performance improvement of array processing through array calibration was also examined.

Keywords: array antenna, array processing, mutual coupling, array uncertainties, GNSS receiver

1. INTRODUCTION

Due to the demands for communication system capacity, spectrum efficiency, and quality improvement in the wireless communication field, an array antenna technique that can detect the direction of radio signals and is capable of beamforming has drawn much attention (Li et al. 2003, Vorobyov et al. 2003). Also, the array antenna technique is considered a core technology for next-generation mobile communication systems, and its importance has increased accordingly. With the recent increase in the jamming of the Global Navigation Satellite Systems (GNSS) around the globe, a technique that can effectively eliminate jamming signals using an array antenna and can precisely acquire/track satellite navigation signals is required in the satellite navigation system field (Seco-Granados et al. 2005, Closas et al. 2009, Arribas et al. 2013, Lee et al. 2016).

Received Jan 27, 2017 **Revised** Mar 22, 2017 **Accepted** Mar 30, 2017
†**Corresponding Author**
E-mail: remero@hanyang.ac.kr
Tel: +82-2-2220-4823 Fax: +82-2-2220-4822

Major national research institutes in many countries, including Centre Tecnológic de Telecommunicacions de Catalunya, have studied satellite navigation signal acquisition/tracking techniques using an array antenna since the mid- to late 2000s (Seco-Granados et al. 2005, Closas et al. 2009, Arribas et al. 2013). However, most of these techniques can only be applied to uniform linear array (ULA) or uniform circular array (UCA) antenna, where each antenna element has an omnidirectional beam pattern and the spacing between the antenna elements is uniform at half of the used signal wavelength, and thus the available range is very limited. The ULA and UCA antennas are the most basic array antenna structures, and the influence between the antenna elements can be minimized when the spacing between the elements is half wavelength. Also, the problem definition as well as the received signal model can be simplified as each antenna element maintains the same beam in every direction. Accordingly, many studies are based on the ULA and UCA antennas.

However, in actual environments, various structures of array antennas are used depending on the environment and purpose of the application field, and each antenna element

generally has a directional beam pattern. In this regard, the beam patterns of the antenna elements could be different from each other. In addition, when the interval between the antenna elements is shorter than half wavelength due to the limitation of the size, the beam pattern of the single antenna element is changed due to the mutual coupling effect from the adjacent antenna elements. The uncertainties of an array antenna such as the position error of the antenna element, in addition to the directional beam pattern and mutual coupling effect, are known to be the factors for deteriorating the performance of the array processing technique (Li et al. 2003, Aksoy & Tuncer 2013, Liao et al. 2013). Therefore, for the design of an actual array system, a signal processing technique considering the uncertainties of an array antenna is essential.

In this study, the performance of the direction detection and beamformer technique depending on the uncertainties of an array antenna was analyzed based on simulation. Also, sector-based array calibration for the alleviation of the uncertainty effect was introduced, and the performance improvement of the array processing technique was examined based on the calibration. By using the actual steering vector obtained through electromagnetic (EM) simulation and the Jahn's channel model (Jahn et al. 1996), which is an experiment-based channel model, the performance of the array processing technique in a realistic environment was investigated.

The contents of this paper are as follows. In Section 2, the signal model is explained; and in Section 3, the array processing technique and the array calibration technique for the alleviation of the array uncertainty effect are explained. In Section 4, the simulation environment and the performance of the array processing technique are analyzed. Lastly, the conclusions of this study are summarized in Section 5.

2. SIGNAL MODEL

2.1 GNSS and Unwanted Signal Models

In this section, the received signal model for an array antenna receiver consisting of M antenna elements is explained. When each navigation satellite periodically transmits its direct sequence spread spectrum (DSSS) signal, the receiver receives the line-of-sight (LOS) signal of DSSS, N_m multipath signals, and the signal where the interference signal and noise have been mixed. The signal received at the front-end of the receiver at time t can be expressed by Eq. (1).

$$\mathbf{y}(\mathrm{t}) = \sum_{\alpha=0}^{N_m} \mathbf{h}_\alpha(t) + \mathbf{g}(t) + \mathbf{u}(t) \tag{1}$$

where $\alpha = 0$ represents the LOS signal, and $\alpha > 0$ represents the multipath signal. The α-th DSSS signal is expressed by Eq. (2).

$$\mathbf{h}_\alpha(t) = A_\alpha(t) q\big(t - \tau_\alpha(t)\big) \cos\big(2\pi f_c t + \phi_\alpha(t)\big)\, \mathbf{a}(\mathbf{\Psi}_\alpha(t)) \tag{2}$$

where $\phi_\alpha(t) = 2\pi f_\alpha(t)^t + \varphi_\alpha(t)$; and $A_\alpha(t)$, $\tau_\alpha(t)$, $f_\alpha(t)$, $\varphi_\alpha(t)$, and $\mathbf{\Psi}_\alpha(t) = [\theta_\alpha(t), \xi_\alpha(t)]^T$ are the strength of the α-th DSSS signal, the time of arrival (TOA), the Doppler frequency, the phase, and the direction of arrival (DOA), respectively. In this regard, the direction of arrival consists of the elevation angle $\theta_\alpha(t)$ and the azimuth angle $\xi_\alpha(t)$. Also, $q(t)$ is the DSSS signal that consists of the navigation message and the inherent spreading code of the satellite (Closas et al. 2009, Lee et al. 2016). f_c is the center frequency of the satellite navigation signal. $\mathbf{a}(\mathbf{\Psi}_\alpha(t))$ is the steering vector, which represents the phase difference between the antenna elements depending on the signal's direction of arrival and the arrangement of the antenna elements. The steering vector is explained in the following section. In Eq. (1), $\mathbf{g}(t)$ and $\mathbf{u}(t)$ are the unknown interference signal and the white noise, excluding the multipath signals.

After the down-conversion, the receiver collects a total of K samples through the sampling period of T_s. In this regard, it is assumed that the wireless channel remains constant during the observation period (KT_s). The baseband received signal sample vector and the received signal sample matrix collected during the n-th observation period are expressed as $\mathbf{y}_n = [\mathbf{y}_{1,n}^T, \mathbf{y}_{2,n}^T, \ldots, \mathbf{y}_{K,n}^T]^T$ and $\mathbf{Y}_n = [\mathbf{y}_{1,n}, \mathbf{y}_{2,n}, \ldots, \mathbf{y}_{K,n}]$, respectively. $\mathbf{y}_{k,n}$ is the k-th baseband received signal sample collected during the n-th observation period, and it can be expressed by Eq. (3).

$$\mathbf{y}_{k,n} = \sum_{\alpha=0}^{N_m} \mathbf{h}_{\alpha,k,n} + \mathbf{g}_{k,n} + \mathbf{u}_{k,n} \tag{3}$$

where $\mathbf{h}_{\alpha,k,n}$, $\mathbf{g}_{k,n}$, and $\mathbf{u}_{k,n}$ represent the $\mathbf{h}_\alpha(t)$, $\mathbf{g}(t)$, and $\mathbf{u}(t)$ after the down-conversion and sampling at time $t = (n\text{-}1)\, KT_s + kT_s$, respectively.

$$\begin{aligned} &A_{\alpha,n} \triangleq A_\alpha(nKT_s), \quad \tau_{\alpha,n} \triangleq \tau_\alpha(nKT_s), \quad \mathbf{\Psi}_{\alpha,n} \triangleq \mathbf{\Psi}_\alpha(nKT_s) \\ &\phi_{\alpha,n} \triangleq \phi_\alpha(nKT_s), \quad q_{\boldsymbol{k}}(\tau_{\alpha,n}) \triangleq q\left((n-1)KT_s + kT_s - \tau_{\alpha,n}\right) \end{aligned} \tag{4}$$

According to Eq. (4), $h_{\alpha,k,n}$ can be expressed by Eq. (5).

$$\mathbf{h}_{\alpha,k,n} = A_{\alpha,n} e^{j\phi_{\alpha,n}} q_k(\tau_{\alpha,n}) \mathbf{a}(\mathbf{\Psi}_{\alpha,n}) = \psi_{\alpha,n} q_k(\tau_{\alpha,n}) \mathbf{a}(\mathbf{\Psi}_{\alpha,n}) \tag{5}$$

https://doi.org/10.11003/JPNT.2017.6.2.43

where $\psi_{\alpha,n} = \mathbf{A}_{\alpha,n}\, e^{j\phi_{\alpha,n}}$ is the complex strength of the signal. $\mathbf{g}_{k,n}$ is differently defined depending on the type of the interference signal. In this study, a single-tone continuous wave (CW) interference signal was assumed. Thus, the interference signal $\mathbf{g}_{k,n}$ is expressed by Eq. (6) (Savasta et al. 2013).

$$\mathbf{g}_{k,n} = \sum_{\beta=1}^{N_i} A_{\beta,n} e^{j2\pi f_{\beta,n}((n-1)KT_S + kT_S)}\, \mathbf{a}(\mathbf{\Psi}_{\beta,n}) \quad (6)$$

where N_i is the total number of interference signals; and $A_{\beta,n}$, $f_{\beta,n}$, and $\mathbf{\Psi}_{\beta,n}$ are the complex strength, frequency offset, and DOA for the β-th interference signal, respectively. It is assumed that the receiver has no information on the interference signal.

2.2 Steering Vector Model

A steering vector refers to the phase difference of an incident signal that is induced by the spatial difference between the antenna elements. For an ideal array antenna where every antenna element has the same omnidirectional beam pattern and there are no uncertainties, the theoretical steering vector for a signal can be defined as the function of the antenna element arrangement and the signal's direction of arrival (Lee & Cheng 2012). For a three-dimensional array antenna consisting of a total of M antenna elements, the theoretical steering vector depending on the incident signal's DOA $\mathbf{\Psi} = [\theta, \xi]^T$ is expressed by Eq. (7).

$$\bar{\mathbf{a}}(\mathbf{\Psi}) = \begin{bmatrix} e^{j\mathbf{p}_1^T\mathbf{k}(\mathbf{\Psi})} \\ e^{j\mathbf{p}_2^T\mathbf{k}(\mathbf{\Psi})} \\ \vdots \\ e^{j\mathbf{p}_M^T\mathbf{k}(\mathbf{\Psi})} \end{bmatrix} \quad (7)$$

where θ and ξ are the elevation angle and azimuth angle of the incident signal, respectively. Also, $j = \sqrt{(-1)}$, $\mathbf{p}_m = [x_m, y_m, z_m]^T$ represents the position vector of the m-th antenna element. $\mathbf{k}(\mathbf{\Psi}) \triangleq \mathbf{k}(\theta, \xi)$ is the propagation vector of the incident signal depending on the DOA, and it is defined by Eq. (8). Fig. 1 shows the example of a three-dimensional array antenna consisting of five elements, and the variables for defining the steering vector are explained.

$$\mathbf{k}(\mathbf{\Psi}) = \mathbf{k}(\theta, \xi) = -\frac{2\pi}{\lambda}\begin{bmatrix} \sin\theta\cos\xi \\ \sin\theta\sin\xi \\ \cos\theta \end{bmatrix} \quad (8)$$

However, for an actual array antenna, the steering vector is defined by Eq. (9) due to the uncertainties such as the position error of the antenna element, anisotropic beam pattern, and mutual coupling (Su & Ling 2001, Aksoy & Tuncer 2013).

$$\mathbf{a}(\mathbf{\Psi}) = \mathbf{C}(\mathbf{\Psi})\bar{\mathbf{a}}(\mathbf{\Psi}) \quad (9)$$

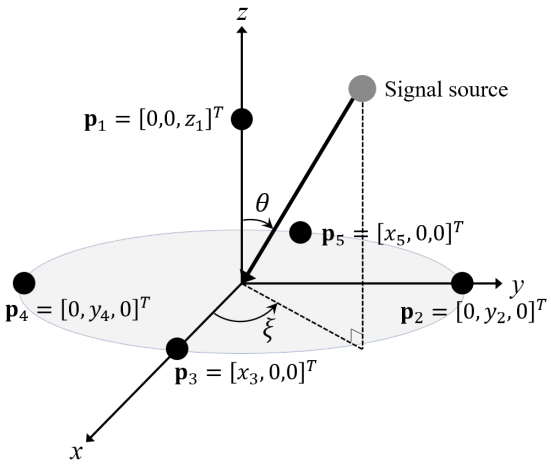

Fig. 1. Example of a 5-element 3-dimensional array antenna.

where $\mathbf{C}(\mathbf{\Psi})$ is the unknown state-transition matrix due to array uncertainties, and it is also called an uncertainty matrix. In an environment without array uncertainties, $\mathbf{C}(\mathbf{\Psi}) = \mathbf{I}_M$. The change in the beam pattern of the antenna element depending on the angle is continuous, and the rate of change is small. Accordingly, it can be assumed that the uncertainty matrix is identical within a certain angle range (Aksoy & Tuncer 2013). Thus, when a total of $D = D_E \times D_A$ sectors are divided depending on the beam pattern of the antenna element, and the angle range of the d-th sector is defined as $\theta \in [\theta_{d,\min}, \theta_{d,\max}]$ and $\xi \in [\xi_{d,\min}, \xi_{d,\max}]$, the uncertainty matrix for the d-th sector can be expressed by Eq. (10).

$$\mathbf{C}_d \triangleq \mathbf{C}(\mathbf{\Psi}) \text{ where } \mathbf{\Psi} = [\theta,\xi]^T, \theta \in [\theta_{d,\min}, \theta_{d,\max}], \xi \in [\xi_{d,\min}, \xi_{d,\max}] \quad (10)$$

where D_E and D_A are the numbers of sectors for the elevation angle and the azimuth angle, respectively.

3. ARRAY PROCESSING TECHNIQUES UNDER UNCERTAINTIES

3.1 Array-Based DOA Estimation

The MUltiple Signal Classification (MUSIC) algorithm (Schmidt 1986) is the most representative technique for estimating the incident signal's DOA using an array antenna. In the MUSIC algorithm, a space spectrum is obtained based on the fact that the signal subspace and the noise subspace are orthogonal to each other, and the signal's DOA is estimated through the peak detection of the spectrum. The signal and noise subspaces can be obtained through the eigen decomposition of the covariance matrix of the received signal.

Based on the orthogonality of the incident signal and the noise, the covariance matrix of the received signal can be defined by Eq. (11).

$$\mathbf{R}_{\mathbf{y},n} = \mathrm{E}[\mathbf{y}_n \mathbf{y}_n^H] = \mathbf{A}_n \mathbf{R}_{\mathbf{s},n} \mathbf{A}_n^H + \sigma_n^2 \mathbf{I}_M \tag{11}$$

where $\mathbf{R}_{\mathbf{s},n}$ and $\sigma_n^2 \mathbf{I}_M$ are the covariance matrix of the incident signal vector and the noise vector; and $\mathbf{I}_M$ is the identity matrix with a size of $M \times M$. In this regard, the matrix $\mathbf{A}_n = [\mathbf{a}(\mathbf{\Psi}_{1,n}), \mathbf{a}(\mathbf{\Psi}_{2,n}), \ldots, \mathbf{a}(\mathbf{\Psi}_{P,n})]$ consists of the steering vectors of P incident signals ($P \leq M$), and $\mathbf{\Psi}_{p,n}$ is the p-th signal's DOA. Through the eigenvalue decomposition of $\mathbf{R}_{\mathbf{y},n}$, the signal and noise subspaces ($\mathbf{E}_{\mathbf{s},n}$ and $\mathbf{E}_{\mathbf{u},n}$) can be obtained. $\mathbf{E}_{\mathbf{s},n} = [\mathbf{e}_{1,n}, \mathbf{e}_{2,n}, \cdots, \mathbf{e}_{P,n}]$ consists of the eigenvectors that correspond to the P largest eigenvalues among the M eigenvalues of $\mathbf{R}_{\mathbf{y},n}$; $\mathbf{E}_{\mathbf{u},n} = [\mathbf{e}_{P+1,n}, \mathbf{e}_{P+2,n}, \ldots, \mathbf{e}_{M,n}]$ consists of the remaining (M-P) eigenvectors. From the noise subspace, the power spectrum of the signal depending on the DOA $\mathbf{\Psi}$ can be calculated using the MUSIC algorithm, as shown in Eq. (12).

$$P_{\mathrm{MUSIC}}(\mathbf{\Psi}) = \frac{1}{\mathbf{a}^H(\mathbf{\Psi}) \mathbf{E}_{\mathbf{u},n} \mathbf{E}_{\mathbf{u},n}^H \mathbf{a}(\mathbf{\Psi})} \tag{12}$$

Using Eq. (12), the power spectrum is calculated for the $\theta \in [0, \pi/2]$ and $\xi \in [0, 2\pi]$ range; and among them, the P largest peak values are estimated to be the incident signal's DOA. In an actual environment, $\mathbf{R}_{\mathbf{y},n}$ is substituted with the sample covariance of the received signal as in Eq. (13).

$$\widehat{\mathbf{R}}_{\mathbf{y},n} = \frac{1}{K} \mathbf{Y}_n \mathbf{Y}_n^H \tag{13}$$

3.2 Array-Based Beamformer

An array antenna receiver can form a beam in the wanted direction by allocating different phases and strengths to each antenna element, and this beam forming technique is called beamforming. The purpose of beamforming is to amplify the signal-to-interference-plus-noise-ratio (SINR) (i.e., to increase the reception rate of the wanted signal) by eliminating or reducing the remaining signal components by adjusting the beam in the direction of the wanted signal. To increase the position determination accuracy of a satellite navigation system receiver, a beam needs to be formed in the direction of the LOS signal (Seco-Granados et el. 2005, Lee et al. 2016).

In the present study, the Capon beamformer (Capon 1969), which is the most representative method, was considered. When the covariance matrix of the multipath/other interference signals and the noise is $\mathbf{R}_{\mathbf{g+u},n}$ as in Eq. (3), the problem of Capon beamformer design can be defined as the problem of maximizing the output SINR of the beamformer, as shown in Eq. (14).

$$\text{maximize} \quad \mathrm{SINR} = \frac{\left|\psi_{0,n}\right|^2 \left|\mathbf{w}^H \mathbf{a}(\mathbf{\Psi}_{0,n})\right|^2}{\mathbf{w}^H \mathbf{R}_{\mathbf{g+u},n} \mathbf{w}} \tag{14}$$

The optimization problem in Eq. (14) can then be interpreted as the problem of minimizing the power of the noise and other interference signals while the strength of the beamformer output in the direction $\mathbf{\Psi}_{0,n}$ is fixed as a constant, as shown in Eq. (15).

$$\begin{aligned} &\text{minimize} \quad \mathbf{w}^H \mathbf{R}_{\mathbf{g+u},n} \mathbf{w} \\ &\text{subject to} \quad \mathbf{w}^H \mathbf{a}(\mathbf{\Psi}_{0,n}) = 1 \end{aligned} \tag{15}$$

For the above optimization problem, the optimal solution can be obtained through the Lagrangian method (Chong & Zak 2013). Accordingly, the Capon beamforming vector is derived as shown in Eq. (16).

$$\mathbf{w}_{MV} = \frac{\mathbf{R}_{\mathbf{g+u},n}^{-1} \mathbf{a}(\mathbf{\Psi}_{0,n})}{\mathbf{a}^H(\mathbf{\Psi}_{0,n}) \mathbf{R}_{\mathbf{g+u},n}^{-1} \mathbf{a}(\mathbf{\Psi}_{0,n})} \tag{16}$$

The Capon beamformer is the problem of mathematically minimizing the covariance matrix, and it is also called a minimum variance beamformer. The Capon beamformer has low complexity and a simple implementation method. However, in an actual environment, the covariance matrix of the noise and the interference signal cannot be calculated. In general, when the number of samples for the received signal is sufficiently larger than the number of antenna elements, the covariance matrix of the noise and the interference signal can be substituted with the sample covariance of the received signal (Li et al. 2003). A GNSS receiver basically performs signal processing by acquiring more than 1,023 samples, and thus, beamforming can be performed using the sample covariance of the received signal as in Eq. (13), as described above.

3.3 Model Mismatch (Array Uncertainties) Effects on Array Processing

As explained earlier, the MUSIC algorithm estimates the incident signal's DOA based on the orthogonality between the signal and noise subspaces. In other words, $\left|\mathbf{A}_{\mathrm{n}}^{\mathrm{H}} \mathbf{E}_{\mathbf{u},n}\right| = \left|[\mathbf{a}(\mathbf{\Psi}_{1,n}), \ldots, \mathbf{a}(\mathbf{\Psi}_{P,n})]^H \mathbf{E}_{\mathbf{u},n}\right| \cong 0$ is satisfied. However, when the uncertainty matrix for the receiver is assumed as $\mathbf{C}(\mathbf{\Psi}_{p,n}) = \mathbf{I}_M$, $\mathbf{a}(\mathbf{\Psi}_{p,n}) = \bar{\mathbf{a}}(\mathbf{\Psi}_{p,n})$ (i.e., the array uncertainties cannot be recognized), model mismatch occurs, and the above equality condition is no longer satisfied. By defining that $\bar{\mathbf{a}}(\mathbf{\Psi}_{p,n}) = \mathbf{a}(\mathbf{\Psi}_{p,n}) + \mathbf{b}_{p,n}$, the fact that $\left|\mathbf{A}_n^H \mathbf{E}_{u,n}\right| \cong 0$ is not valid, on

the assumption of $\mathbf{C}(\mathbf{\Psi}_{p,n}) = \mathbf{I}_M$, can be seen in Eq. (17).

$$\left|\left[\mathbf{a}(\mathbf{\Psi}_{1,n}) + \mathbf{b}_{1,n}, \cdots, \mathbf{a}(\mathbf{\Psi}_{P,n}) + \mathbf{b}_{P,n}\right]^H \mathbf{E}_{\mathbf{u},n}\right| = \left|\left[\mathbf{b}_{1,n}, \cdots, \mathbf{b}_{P,n}\right]^H \mathbf{E}_{\mathbf{u},n}\right| \neq 0 \quad (17)$$

where $\mathbf{b}_{p,n}$ is the bias error vector of the steering vector for the p-th signal. Thus, when the DOA is estimated using a steering vector that is different from the actual steering vector, the estimation of the DOA includes an error. Similarly, for the beamformer, the model mismatch of the steering vector forms a beam in a direction that is different from the look direction, and also deteriorates the beamformer output SINR. Therefore, to prevent the performance deterioration of the array processing technique in a system with array uncertainties, the estimation of the actual steering vector should be enabled by accurately estimating the array uncertainty matrix.

3.4 Array Calibration

Array calibration is a technique that alleviates the model mismatch effect of the steering vector by estimating the uncertainty matrix or the actual steering vector. Depending on the reference data acquisition method of the array antenna, it is classified into pilot calibration, self-calibration, adaptive calibration, and active calibration. Detailed explanations on each technique can be found in Willerton 2013. As the present study focuses on the performance analysis of array processing depending on array uncertainties and calibration, only the pilot calibration, which is the most representative calibration technique, was considered. In the pilot calibration, based on the relationship between the theoretical steering vector and the actual steering vector (refer to Eqs. (9) and (10)), the problem of uncertainty vector estimation for each sector is defined as shown in Eq. (18).

$$\begin{aligned} &\underset{\mathbf{C}_d}{\text{minimize}} \quad \|\mathbf{A}_d - \mathbf{C}_d\bar{\mathbf{A}}_d\|^2 \\ &\text{subject to} \quad \mathbf{\Psi} = [\theta, \xi]^T, \theta \in \left[\theta_{d,\min}, \theta_{d,\max}\right], \xi \in \left[\xi_{d,\min}, \xi_{d,\max}\right] \end{aligned} \quad (18)$$

where $\mathbf{A}_d = [\mathbf{a}(\mathbf{\Psi}_{d,\min}), \ldots, \mathbf{a}(\mathbf{\Psi}_{d,\max})]$ is a set of steering vectors acquired through a far field pilot source-based experiment or EM simulation, and $\bar{\mathbf{A}}_d = [\bar{\mathbf{a}}(\mathbf{\Psi}_{d,\min}), \ldots, \bar{\mathbf{a}}(\mathbf{\Psi}_{d,\max})]$ is a set of theoretical steering vectors corresponding to $\mathbf{A}_d$. Also, $\mathbf{\Psi}_{d,\min} = [\theta_{d,\min}, \xi_{d,\min}]^T$ and $\mathbf{\Psi}_{d,\max} = [\theta_{d,\max}, \xi_{d,\max}]^T$.

From Eq. (18), the uncertainty matrix can be estimated as shown in Eq. (19) based on the least squares estimation (Su & Ling 2001).

$$\begin{aligned} &\hat{\mathbf{C}}_d = \hat{\mathbf{C}}(\mathbf{\Psi}) = \mathbf{A}_d\bar{\mathbf{A}}_d^H\left[\bar{\mathbf{A}}_d\bar{\mathbf{A}}_d^H\right]^{-1} \\ &\text{where } \mathbf{\Psi} = [\theta, \xi]^T, \theta \in \left[\theta_{d,\min}, \theta_{d,\max}\right], \xi \in \left[\xi_{d,\min}, \xi_{d,\max}\right] \end{aligned} \quad (19)$$

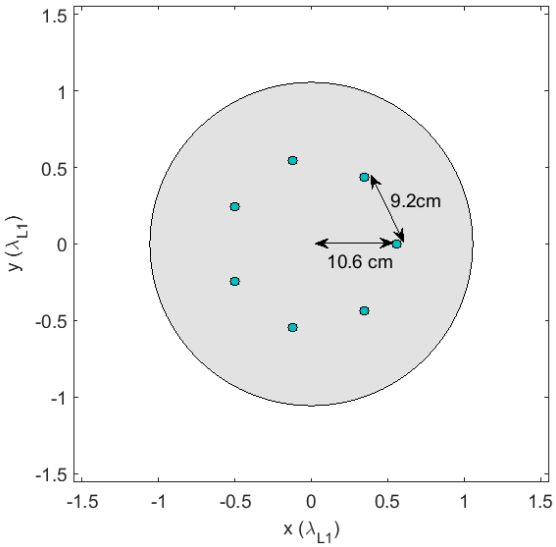

Fig. 2. 7-element UCA for GPS L1/L2 (Byun & Choo under review).

Based on this, the actual steering vector for each sector can be estimated.

$$\begin{aligned} &\hat{\mathbf{a}}(\mathbf{\Psi}) = \hat{\mathbf{C}}(\mathbf{\Psi})\bar{\mathbf{a}}(\mathbf{\Psi}) \\ &\text{where } \mathbf{\Psi} = [\theta, \xi]^T, \theta \in \left[\theta_{d,\min}, \theta_{d,\max}\right], \xi \in \left[\xi_{d,\min}, \xi_{d,\max}\right] \end{aligned} \quad (20)$$

4. PERFORMANCE EVALUATION

4.1 Simulation Settings

In this section, the performance of array processing based on the 7-element UCA for GPS L1/L2 (Byun & Choo under review) was analyzed. The 7-element UCA consists of seven identical directional antenna elements (Amotech Co. Ltd. 2017). The radius of the array antenna is 10.6 cm (0.5566 λ_{L1}), and the spacing between the antenna elements is 9.2 cm (0.483 λ_{L1}). λ_{L1} = 19 cm represents the wavelength of the GPS L1 signal. Fig. 2 shows the shape of the array antenna. For the GPS L1 signal, the spacing between the antenna elements is shorter than the half wavelength of the signal, and thus, there is mutual coupling effect between the adjacent antenna elements. Accordingly, the actual steering vector is different from the theoretical steering vector. Based on EM simulation, the actual steering vector was measured at 1 degree intervals for elevation angles of 0~90 degrees and azimuth angles of 0~359 degrees.

Table 1 summarizes the simulation environment. The GPS L1 C/A signal was used for the simulation, and the performance of array processing depending on the CW jamming was analyzed. To configure a channel that is similar to an actual environment, the Jahn's channel model,

Table 1. Simulation environment.

Parameter	Value	Remark
Received signals	GPS L1 C/A signal Continuous-wave signals	LOS signal incident from (20,120) degrees Jamming signals incident from random directions
Channel model	Jahn's channel	Experimental model; Multipath signals are generated in terms of the DOA of the LOS signal.
CNR	45 dB-Hz	Corresponding SNR: -18 dB
JSR	-40 dB	-
Sampling rate	4.092 MHz	-

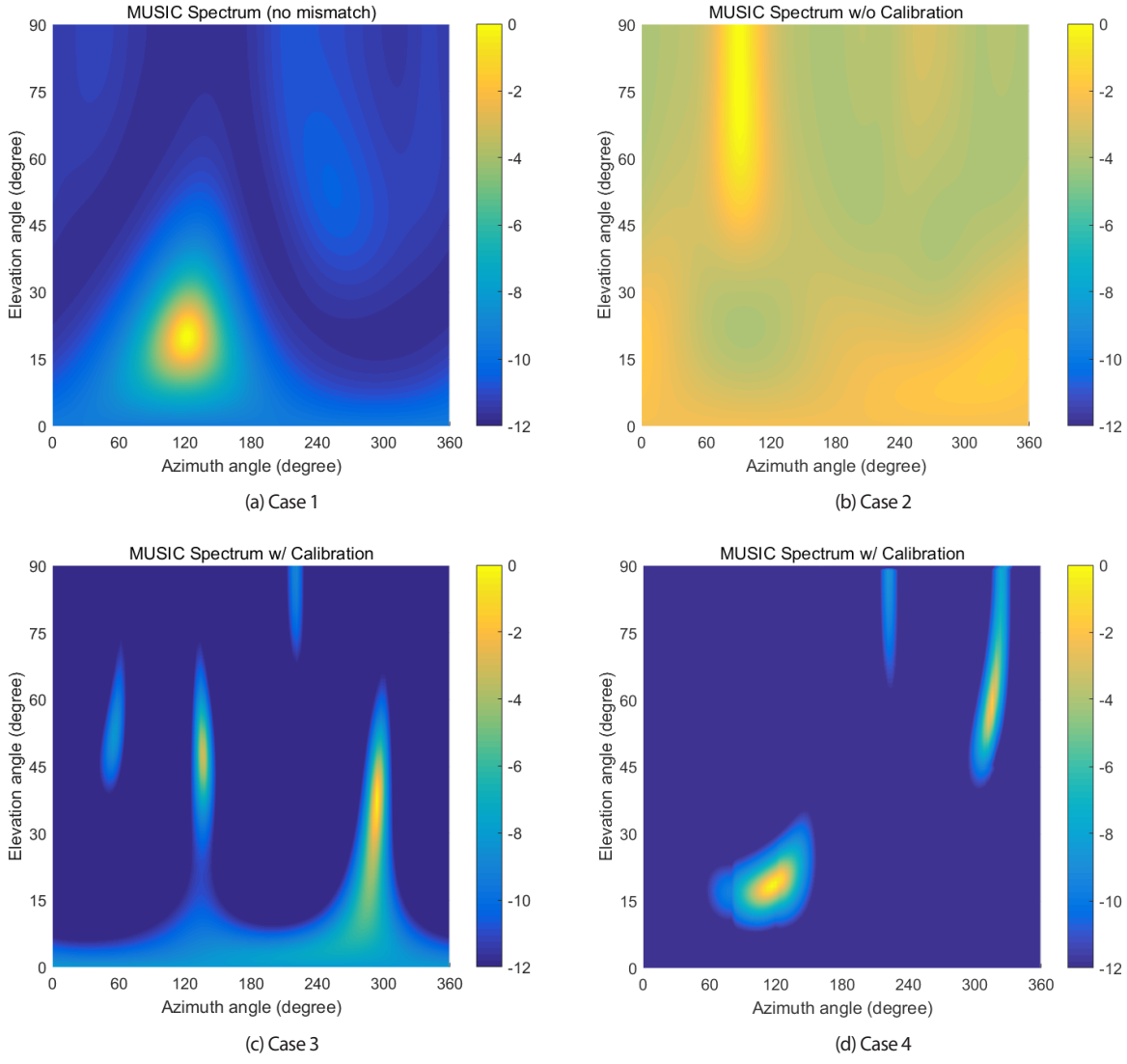

Fig. 3. Power spectrum for each direction based on the MUSIC algorithm.

which is an experimental channel model, was used (Jahn et al. 1996). The number of multipath signals and their strengths were determined through the Jahn's channel model. Also, the carrier-to-noise ratio (CNR) was set to 45 dB-Hz; and the jammer-to-signal ratio (JSR) was set to -40 dB. The sampling rate of the receiver was assumed to be 4.092 MHz, which is four times the chip rate of the GPS L1 C/A signal (1.023 MHz). To examine the effect of the steering vector model mismatch depending on array uncertainties and the effect of the array calibration, simulations were performed for the following cases based on the same environment.

Case 1: There is no steering vector model mismatch (array

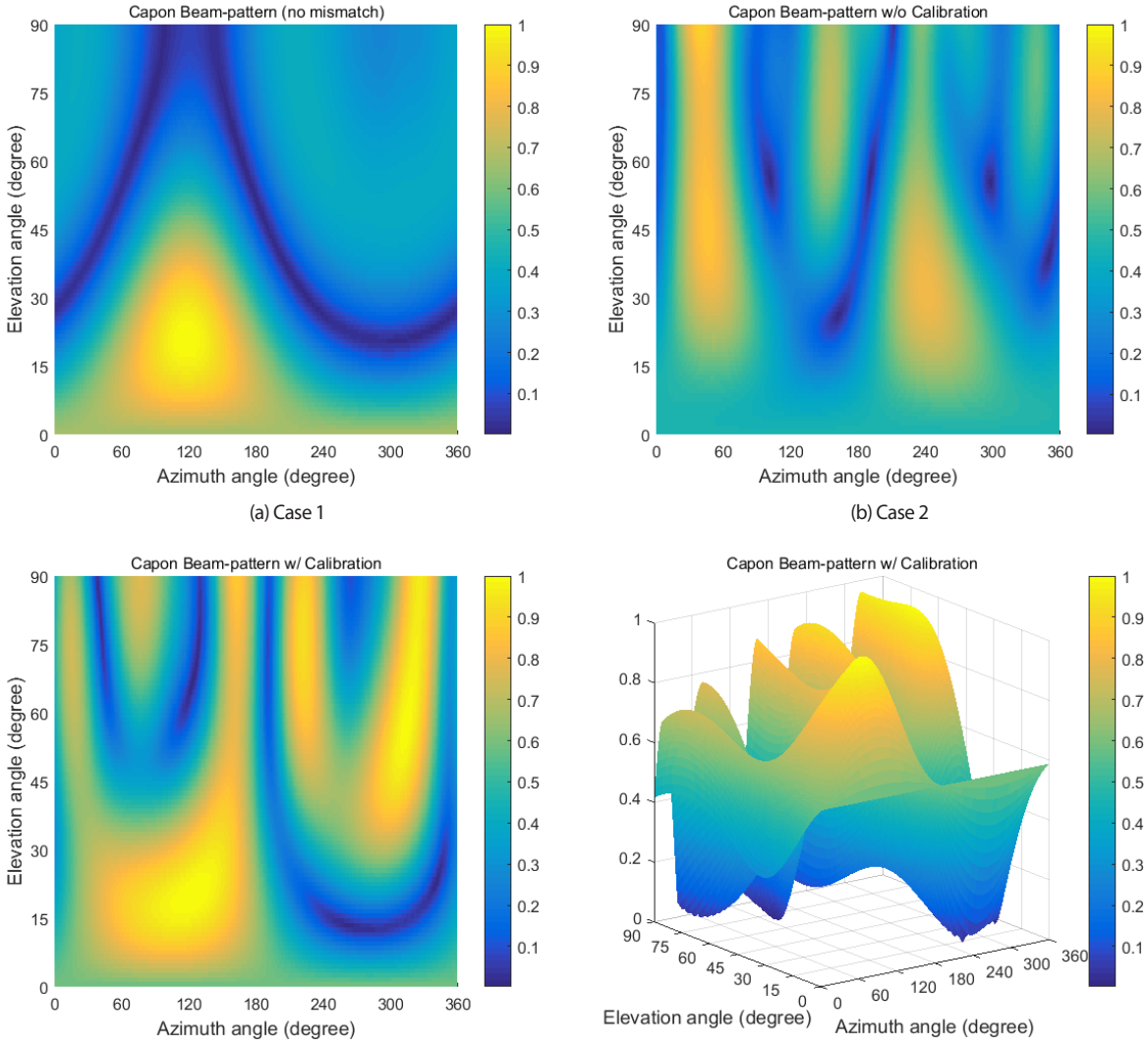

Fig. 4. Beam pattern of the Capon beamformer.

uncertainties) (i.e., $\mathbf{C}(\mathbf{\Psi}) = \mathbf{I}_M$).

Case 2: There is steering vector model mismatch, but $\mathbf{C}(\mathbf{\Psi})$ is not known.

Case 3: There is steering vector model mismatch, and $\mathbf{C}(\mathbf{\Psi})$ is estimated through array calibration (For the array calibration, it is assumed that $D = 1$).

Case 4: There is steering vector model mismatch, and $\mathbf{C}(\mathbf{\Psi})$ is estimated through array calibration (For the array calibration, it is assumed that $D = 18$, $D_E = 9$, $D_A = 2$).

In Case 1, the actual steering vector was produced through the theoretical steering vector model (refer to Eq. (7)); and in Cases 2-4, the actual steering vector was measured through EM simulation.

4.2 Simulation Results

Fig. 3 shows the power spectrum depending on the direction in an environment without electronic interference (jamming and multipath signals), based on the MUSIC algorithm. When there was no steering vector model mismatch (Case 1), the direction of the GPS L1 C/A signal could be accurately detected through the MUSIC algorithm, as shown in the figure. However, when there was steering vector model mismatch and no array calibration (Case 2), false detection occurred, which indicated that the signal was received from a completely different direction. When the sector division for array calibration was insufficient (Case 3), the direction of the incident signal could not be detected, either. In Case 4, the main lobe of the power spectrum was formed in the direction of the GPS L1 C/A signal, and thus, the direction of the incident signal could be detected

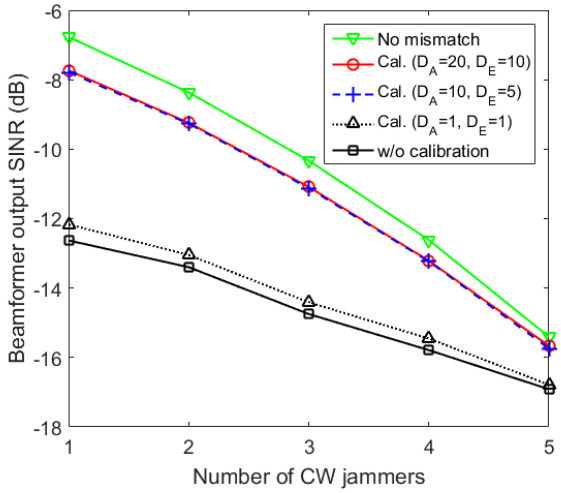

Fig. 5. Output SINR of the Capon beamformer.

through the array calibration. However, a side lobe was formed due to the array calibration error, indicating that the direction detection rate could deteriorate depending on the environment (i.e., signal strength relative to noise).

Fig. 4 shows the beam pattern of the Capon beamformer. For the analysis of the beam pattern, it was assumed that the look direction is identical to the direction of the GPS L1 C/A signal. In Case 1, a main lobe was formed exactly in the look direction. However, in Case 2, a beam was formed in the direction that is completely different from the look direction, and thus, the beamformer function was limited due to the steering vector model mismatch. In Case 4, a main lobe could be formed in the look direction through the array calibration, but a side lobe was formed due to the array calibration error, as shown in Fig. 3. When there is an interference signal in the direction of the side lobe, the reception SINR could deteriorate significantly.

To analyze the output SINR of the Capon beamformer, Monte Carlo simulation was carried out 2,000 times. For the simulation, the direction of the GPS L1 C/A signal was fixed (Table 1), and the direction of the jamming signal was set to random, but it was made to be at least 20 degrees apart from the direction of the LOS signal. Fig. 5 shows the output SINR of the Capon beamformer depending on the number of jamming signals and the number of sectors for array calibration. When the array calibration was performed in more detail, the output SINR increased. In general, the output SINR decreased as the number of jamming signals increased. This is because the effect of the interference signal remained due to the side lobe formation depending on the array calibration error.

5. CONCLUSIONS

In this study, the performance of array processing depending on the array uncertainties (e.g., mutual coupling between antenna elements, position error of the antenna element, and anisotropic beam pattern) was analyzed through simulation, along with the performance of array processing depending on the pilot-based array calibration in an array uncertainty environment. To implement a simulation environment that is similar to an actual environment, the actual steering vector of 7-element UCA was measured through EM simulation, and the Jahn's channel model was used. The analysis of the power spectrum and beam pattern for each direction showed that the direction detection and interference elimination performance was limited due to the array uncertainties, and the performance was improved through the array calibration. In addition, the analysis of the beamformer output SINR showed that higher performance could be obtained when the array calibration was conducted in more detail. In the future, studies on the minimization of the side lobe effect through the reduction of the array calibration error need to be conducted.

ACKNOWLEDGMENTS

This work was supported by ICT R&D program of MSIP/IITP (2014-044-052-001, Development of Verification Platform Technologies for GNSS Signal Interference).

REFERENCES

Aksoy, T. & Tuncer, T. E. 2013, Sectorized approach and measurement reduction for mutual coupling calibration of non-omnidirectional antenna arrays, Radio Science, 48, 102-110. http://dx.doi.org/10.1002/rds.20017

Amotech Co. Ltd. website, GPS Patch Pin Type Antenna: B25-2D02753-STD70, [Internet], cited 2017 March 31, available from: http://www.amotech.co.kr/Eng/KST/ProductView.asp?n=68

Arribas, J., Fernandez-Prades, C., & Closas, P. 2013, Multi-antenna techniques for interference mitigation in GNSS signal acquisition, EURASIP Journal on Advances in Signal Processing, 2013:143. http://dx.doi.org/10.1186/1687-6180-2013-143

Byun, G. & Choo, H. under review, A novel approach to array manifold calibration using single-direction information for accurate direction-of-arrival estimation, IEEE Transactions on Antennas and Propagation.

Capon, J. 1969, High-resolution frequency-wavenumber

spectrum analysis, Proceedings of the IEEE, 57, 1408-1418. http://dx.doi.org/10.1109/PROC.1969.7278

Chong, E. K. P. & Zak, S. H. 2013, An Introduction to Optimization, 4th ed. (New Jersey: John Wiley & Sons).

Closas, P., Fernandez-Prades, C., & Fernandez-Rubio, J. A. 2009, A Bayesian approach to multipath mitigation in GNSS receivers, IEEE Journal of Selected Topics in Signal Processing, 3, 695-706. http://dx.doi.org/10.1109/JSTSP.2009.2023831

Jahn, A., Bischl, H., & Heiss, G. 1996, Channel characterization for spread spectrum satellite communications, in Proceedings of IEEE 4th International Symposium on Spread Spectrum Techniques and Application, Mainz, Germany, 22-25 Sept. 1996. http://dx.doi.org/10.1109/ISSSTA.1996.563500

Lee, J.-H. & Cheng, C.-C. 2012, Spatial correlation of multiple antenna arrays in wireless communications systems, Progress in Electromagnetics Research, 132, 347-368. http://dx.doi.org/10.2528/PIER12080604

Lee, S., Lohan, E. S., & Kim, S. 2016, Array-based GNSS signal tracking with a reduced state signal model, IEEE Transactions on Aerospace and Electronic Systems, 52, 1267-1283. http://dx.doi.org/10.1109/TAES.2016.150024

Li, J., Stoica, P., & Wang, Z. 2003, On robust Capon beamforming and diagonal loading, IEEE Transactions on Signal Processing, 51, 1702-1715. http://dx.doi.org/10.1109/TSP.2003.812831

Liao, B., Chan, S.-C., & Tsui, K.-M. 2013, Recursive steering vector estimation and adaptive beamforming under uncertainties, IEEE Transactions on Aerospace and Electronic Systems, 49, 489-501. http://dx.doi.org/10.1109/TAES.2013.6404116

Savasta, S., Presti, L. L., & Rao, M. 2013, Interference mitigation in GNSS receivers by a time-frequency approach, IEEE Transactions on Aerospace and Electronic Systems, 49, 415-438. http://dx.doi.org/10.1109/TAES.2013.6404112

Schmidt, R. O. 1986, Multiple emitter location and signal parameter-estimation, IEEE Transactions on Antennas and Propagation, AP-34, 276-280. http://dx.doi.org/10.1109/TAP.1986.1143830

Seco-Granados, G., Fernandez-Rubio, J. A., & Fernandez-Prades, C. 2005, ML estimator and hybrid beamformer for multipath and interference mitigation in GNSS receivers, IEEE Transactions on Signal Processing, 53, 1194-1208. http://dx.doi.org/10.1109/TSP.2004.842193

Su, T. & Ling, H. 2001, On modeling mutual coupling in antenna arrays using the coupling matrix, Microwave and Optical Technology Letters, 28, 231-237.

Vorobyov, S. A., Gershman, A. B., & Luo, Z.-Q. 2003, Robust adaptive beamforming using worst-case performance optimization: A solution to the signal mismatch problem, IEEE Transactions on Signal Processing, 51, 313-324. http://dx.doi.org/10.1109/TSP.2002.806865

Willerton, M. 2013, Array auto-calibration, PhD Dissertation, Imperial College London. http://hdl.handle.net/10044/1/11684

Sangwoo Lee received the B.S. and M.S. degrees both in Electrical Engineering from Ajou University, Suwon, Korea in 2009 and 2011, and the Ph.D. degree in Electronics and Computer Engineering from Hanyang University, Seoul, Korea in 2016. He is currently a senior researcher at Korea Aerospace Research Institute, Daejeon, Korea. His research interests include wireless localization, signal processing and network strategies for positioning purposes.

Moon-Beom Heo received a M.S. and Ph.D. degrees in Mechanical and Aerospace Engineering from the Illinois Institute of Technology. He is currently a head of the satellite navigation team at Korea Aerospace Research Institute, Daejeon, Korea. His work is focused on satellite navigation systems.

Cheonsig Sin was born in Ok-cheon, Korea on Sept. 10, 1964. He joined Electronics and Telecommunication Research Institutes (ETRI) in 1990. From 1990 to 2006, he served as a research associate at ETRI where he investigated the satellite frequency & orbit coordination and the satellite system design. He worked for the GPS and Galileo receiver R&D division of ETRI from 2007 to 2010. He is in charge of development for GNSS Interference Verification Platform technology. His research interests include GNSS system and infrastructures.

Sunwoo Kim received a B.S. in Electrical Engineering from Hanyang University, Seoul, Korea in 1999, and M.S. and Ph.D. degrees in Electrical and Computer Engineering from the University of California, Santa Barbara, U.S.A. in 2002 and 2005, respectively. He is currently an associate professor in the Department of Electronics Engineering, Hanyang University, Seoul, Korea. His research interests include signal processing, wireless communications, wireless networks, and 5G networks.